ISSN 1063-7761, Journal of Experimental and Theoretical Physics, 2006, Vol. 102, No. 5, pp. 799–809. © Pleiades Publishing, Inc., 2006.
Original Russian Text © A.V. Shaposhnikov, D.V. Gritsenko, I.P. Petrenko, O.P. Pchelyakov, V.A. Gritsenko, S.B. Érenburg, N.V. Bausk, A.M. Badalyan, Yu.V. Shubin, T.P. Smirnova, H. Wong, C.W. Kim, 2006, published in Zhurnal Éksperimental'noĭ i Teoreticheskoĭ Fiziki, 2006, Vol. 129, No. 5, pp. 914–925.

ELECTRONIC PROPERTIES OF SOLIDS

The Atomic and Electron Structures of ZrO_2

A. V. Shaposhnikov[a],*, D. V. Gritsenko[a], I. P. Petrenko[a], O. P. Pchelyakov[a], V. A. Gritsenko[a], S. B. Érenburg[b], N. V. Bausk[b], A. M. Badalyan[b], Yu. V. Shubin[b], T. P. Smirnova[b], H. Wong[c], and C. W. Kim[d]

[a] *Institute of Semiconductor Physics, Siberian Division, Russian Academy of Sciences, Novosibirsk, 630090 Russia*
[b] *Institute of Inorganic Chemistry, Siberian Division, Russian Academy of Sciences, Novosibirsk, 630090 Russia*
[c] *Electronic Engineering Department, City University of Hong Kong, Hong Kong*
[d] *Samsung Advanced Institute of Technology, P.O. Box 111, Suwon 440-600, Korea*
**e-mail: shaposh@isp.nsc.ru*

Received October 18, 2005

Abstract—The atomic structure of amorphous and crystalline zirconium dioxide (ZrO_2) films was studied using X-ray diffraction and extended X-ray absorption fine structure techniques. The electron structure of ZrO_2 was experimentally determined using X-ray and UV photoelectron spectroscopy, and the electron energy band structure was theoretically calculated using electron density functional method. According to these data, the valence band of ZrO_2 consists of three subbands separated by an ionic gap. The upper subband is formed by the O2*p* states and Zr4*d* states; the medium subband is formed by the O2*s* states; and the narrow lower subband is formed predominantly by the Zr4*p* states. The bandgap width in amorphous ZrO_2, as determined using the electron energy loss spectroscopy data, amounts to 4.7 eV. The electron band structure calculations performed for a cubic ZrO_2 phase point to the existence of both light ($0.3m_0$) and heavy ($3.5m_0$) holes, where m_0 is the free electron mass. The effective masses of band electrons in ZrO_2 fall within $(0.6–2.0)m_0$.

PACS numbers: 71.15.Mb, 71.20, 73.61.Ng, 77.22.-d

DOI: 10.1134/S1063776106050128

1. INTRODUCTION

In silicon field-effect transistors, a reduction of the channel length to about 600 Å is accompanied by scaling-related decrease in the SiO_2 gate insulator thickness down to 12 Å. As a result, the tunneling current through such a thin SiO_2 layer increases to unacceptable level that leads to excess power dissipation. The main approach to solution of this problem consists in replacing SiO_2 by so-called alternative insulators with higher values of the dielectric constant, which are also referred to as high-*k* gate dielectrics [1–3]. Another important application of these high-*k* materials is related to their use as insulators in capacitors of dynamic random access memories [2, 3]. The third use of alternative dielectrics is in top insulators of FLASH memory elements [4, 5].

At present, materials extensively studied as alternative gate dielectrics include hafnium dioxide (HfO_2, $\varepsilon = 25$), zirconium dioxide (ZrO_2, $\varepsilon = 25$), yttrium oxide (Y_2O_3, $\varepsilon = 15$), and aluminum oxide (Al_2O_3, $\varepsilon = 10$). Among these, one of the most promising is ZrO_2 that possesses a broad bandgap and exhibits high barriers for electron and hole injection at the Si/ZrO_2 interface [2, 3]. While the atomic and electron structures of SiO_2 and Si_3N_4—the two key dielectrics used in modern semiconductor devices—have been studied in much detail [6, 7], profound investigations of the atomic and electron structures of the aforementioned alternative dielectrics, including ZrO_2, have just started.

At atmospheric pressure, zirconium dioxide exists in an amorphous state and in three crystalline polymorphous modifications [8]. In the low-temperature range ($T < 1400$ K), the most stable is the monoclinic C_{2h}^5 polymorph (space group, $P2_1/c$); at elevated temperatures (1400–2600 K), the tetragonal D_{4h}^{15} polymorph (space group, $P4_2/nmc$); and above 2600 K, the cubic O_h^5 polymorph (space group, $Fm3m$). In the cubic and tetragonal phases, the coordination number of oxygen and zirconium atoms are 4 and 8, respectively. In the monoclinic phase, there are oxygen atoms of the two types with the coordination numbers 3 and 4, and the coordination number of zirconium is 7.

Under normal conditions (room temperature and atmospheric pressure), crystalline ZrO_2 exists in the monoclinic modification. The cubic phase can be stabilized at low temperatures by adding impurities such as Ca, Mg, and Y [9]. It was reported [10–13] that cubic modifications were formed in thin (100- to 500-Å-thick) ZrO_2 and HfO_2 films at temperatures

about 200°C. At 300–600°C, these films adopted tetragonal modifications with the parameters that were significantly different from those of the corresponding high-temperature volume phases. The formation of a stable monoclinic phase was observed in films with thicknesses above 500 Å.

One of the most important problems related to metal–oxide–silicon (MOS) structures is the excess leakage current at the Si/dielectric interface. At room temperature, the injection of carriers at such interfaces with barriers within 1.5–4.0 eV proceeds according to the Fowler–Nordheim mechanism, whereby the tunneling injection current is exponentially dependent on the effective mass (m^*) of charge carriers in the dielectric [14, 15]. According to the results of energy band calculations and experimental data for SiO_2 and si_3N_4, these dielectrics contain “light” electrons with effective masses $m_e^* \approx (0.3–1.4)m_0$, where m_0 is the free electron mass [15–19]. At the same time, the holes in these materials are “heavy,” possessing effective masses within $m_h^* \approx (2.5–10)m_0$ [16–18]. The presence of such heavy holes is related to a narrowband of nonbonding $O2p_\pi$ orbitals in SiO_2 and $N2p_\pi$ orbitals in Su_3O_4. To our knowledge, the effective masses of electrons and holes in ZrO_2 have not been theoretically or experimentally studied so far.

The aims of the present investigation was to characterize the atomic and electron structures of ZrO_2 using experimental and theoretical methods and evaluate the effective masses of electrons and holes in this dielectric.

2. EXPERIMENTAL METHODS

ZrO_2 films with thicknesses in the range from 200 to 600 Å were deposited by sputtering a metallic zirconium target (99% Zr) in an argon–oxygen mixture in a plasma deposition setup of the ARC-12M type. The films were deposited at 150° onto ⟨100⟩ -oriented n-Si single crystal substrates with a resistivity of about 20 Ω cm. Prior to deposition, the substrates were subjected to the standard chemical treatment. Then, the vacuum chamber was evacuated to a residual pressure of 10^{-8} Torr and an argon–oxygen mixture was admitted to the chamber at a component flux ratio of 2 : 23. During the deposition of ZrO_2 films, the dynamic pressure in the chamber was maintained on a level of 10^{-3} Torr. In order to obtain crystalline ZrO_2 films, a fraction of the samples were annealed at 800°C for 30min in air at atmospheric pressure.

The sample film structure was studied by X-ray diffraction using synchrotron radiation with a wavelength of $\lambda = 1.5406$ Å. The diffraction patterns were obtained on a high-resolution diffractometer at the Budker Institute of Nuclear Physics (Siberian Division of the Russian Academy of Sciences, Novosibirsk). The measurements were performed using a grazing incidence geometry ($\theta \approx 4°$) with a sample rotated around the normal to the film surface. The diffractograms were recorded by scanning the angular interval $2\theta = 20–70°$ with a step of $\Delta(2\theta) = 0.05°$.

The measurements of extended X-ray absorption fine structure (EXAFS) of ZrK radiation in ZrO_2 films were performed in the Budker Institute of Nuclear Physics (Novosibirsk), using synchrotron radiation from a VEPP-3 storage ring operating at an electron energy of 2 GeV and a beam current of 50–100 mA. The radiation was monochromated by two-crystal monochromator based on a monoblock cut ⟨111⟩-oriented silicon single crystal and detected using an ionization chamber filled with an Ar/H mixture. The EXAFS spectra were recorder using a surface-sensitive fluorescence technique for determining the X-ray absorption coefficient. This technique is based on measurements of the intensity of the secondary (fluorescent) emission generated upon decay of an excited hole state of an atom with a vacancy on a core level, which appears as a result of the absorption of an X-ray quantum. The intensity of such processes is proportional to the frequency of hole production and, hence, to the X-ray absorption coefficient. In order to eliminate the influence of the monochromatic synchrotron radiation reflected from the substrate, a table holding the sample was rotated at a frequency of 10–15 Hz. The EXAFS data were processed using EXCURV92 program package [20]. The phase and amplitude characteristics were calculated in the Xα-DW approximation using special procedures stipulated by this program package. The local atomic environment was analyzed using a procedure of the Fourier-filtered data fitting with the weight $k\chi(k)$, where k is the wavevector and $\chi(k)$ is the normalized oscillating part of the absorption coefficient. The fitting was performed in the interval of photoelectron wavevectors from 3 to 12 A^{-1}.

The X-ray (XPS) and UV (UPS) photoelectron spectra were measured on an ESCALAB 220i-XL spectrometer (Vacuum Generators, England) using monochromated AlK_α radiation with a quantum energy of $E = 1.486.6$ eV and helium plasma with $E = 21.2$ eV (HeI) and 40.8 eV (HeII).

The electron energy loss spectroscopy (EELS) measurements were performed using a LAS-3000 Auger electron spectrometer (Riber, France) with an electron energy analyzer of the cylindrical mirror type with a 0.25% resolution. The EELS spectra were recorded using the primary electron beam with an energy varied within $E = 200–500$ eV. The electron beam was incident on the sample surface at an angle of 90°, and the reflected electrons were detected at an angle of 43°.

MOS (Al–ZrO_2–Si) structures for the electric measurements were prepared by depositing ZrO_2 films onto ⟨100⟩-oriented n- and p-Si single crystal substrates with a resistivity of about 10 Ω cm. The thickness of a ZrO_2 layer was determined by ellipsometry using He–Ne

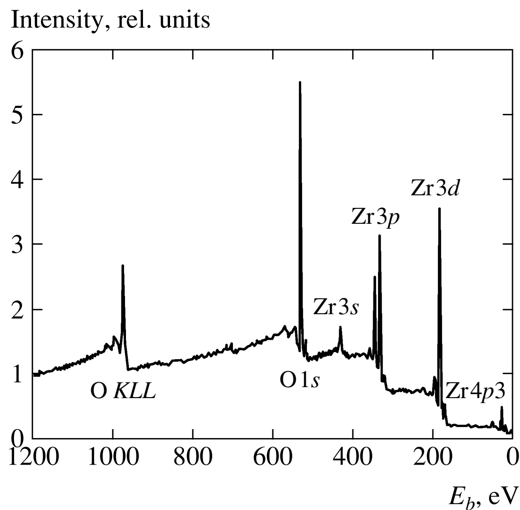

Fig. 1. Review XPS spectrum of an amorphous ZrO_2 film.

laser radiation with $\lambda = 6328$ Å. The metal contact with an area of 5×10^{-3} cm^2 was formed by depositing aluminum in vacuum via a mask.

3. ATOMIC STRUCTURE OF ZrO_2 FILMS BY X-RAY DIFFRACTION AND EXAFS DATA

Figure 1 presents a review XPS spectrum of an amorphous ZrO_2 film. An analysis of the relative intensities of Zr3*d* and O1*s* photoelectron peaks showed that the chemical composition of deposited amorphous zirconium dioxide coincides to within 5% with the stoichiometric formula of ZrO_2.

According to the X-ray diffraction data, the vacuum-annealed crystalline ZnO_2 films had a cubic structure with a lattice parameter of a = 5.07 Å. Figure 2 shows the typical X-ray diffractograms of ZrO_2 films in the as-deposited and annealed (800°C, 30 min) states in comparison to the diffractogram of a powdered cubic ZrO_2. The formation of a high-temperature cubic structure as a result of the annealing at 800°C can be explained by the existence of a thermodynamically nonequilibrium amorphous modification of ZrO_2 in the initial (as-deposited) state. Apparently, a stable monoclinic modification can be obtained using more prolonged annealing, since the high-temperature structure

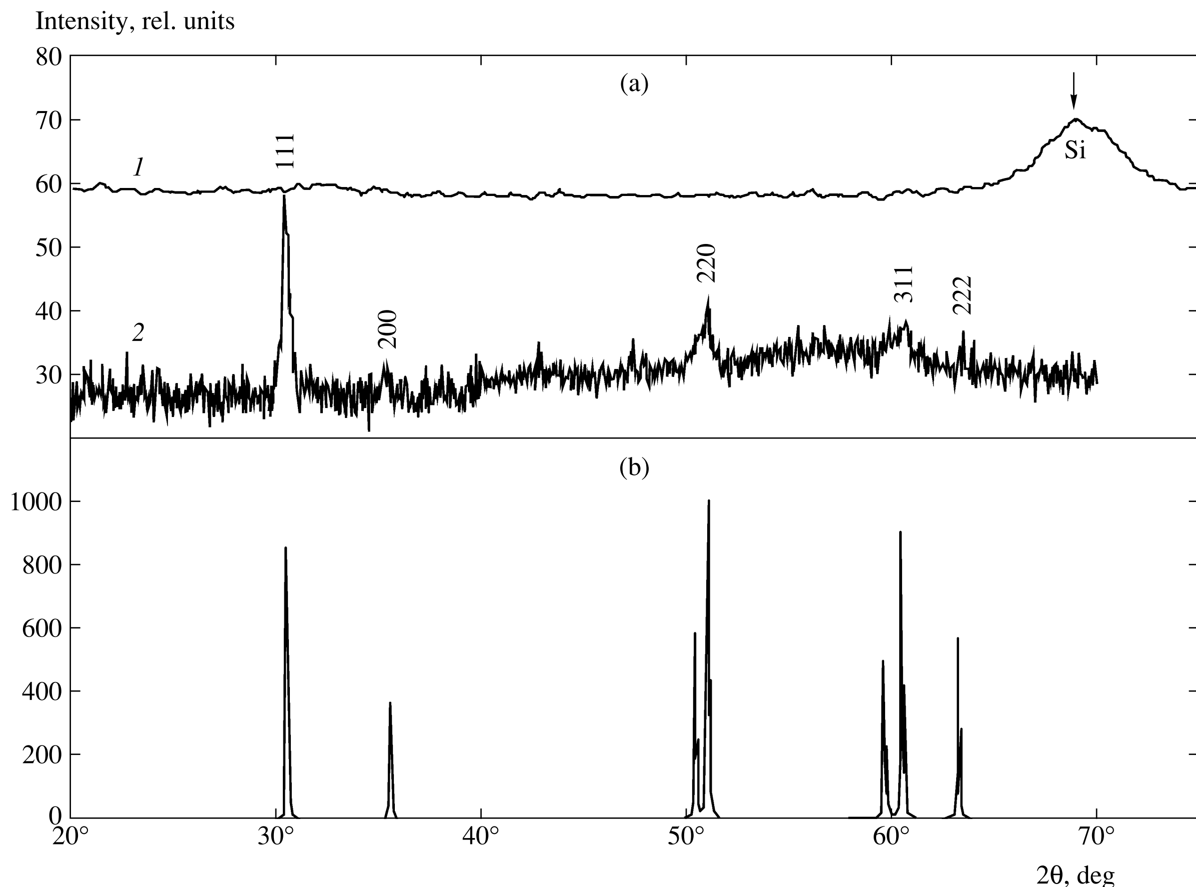

Fig. 2. X-ray diffractograms of (a) ZrO_2 films in (*1*) freshly deposited and (*2*) annealed (800°C, 30 min) states and (b) cubic ZrO_2 powder.

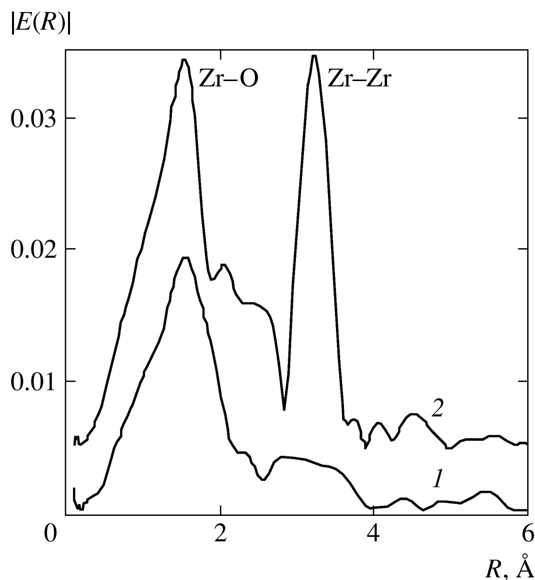

Fig. 3. Radial distribution function by EXAFS of Zr*K* radiation for ZrO_2 films in (*1*) freshly deposited and (*2*) annealed (800°C, 30 min) states.

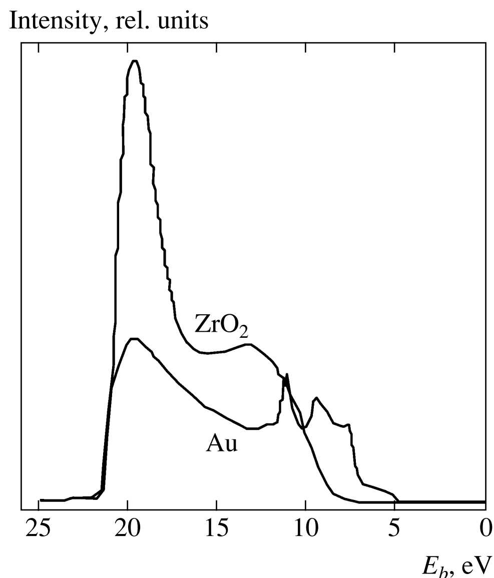

Fig. 4. UPS spectra of an amorphous ZrO_2 film and Au excited by HeI radiation ($E = 21.2$ eV).

exhibits a reverse transition to the monoclinic structure at temperatures below 1050°C.

Figure 3 shows the moduli of the Fourier transform of the $k^2\chi(k)$ function in the EXAFS spectrum of Zr*K* radiation (radial structure functions without phase corrections) for ZrO_2 films before and after vacuum annealing. As can be seen, the initial film is completely amorphous (the peaks corresponding to Zr–Zr distances are absent). The annealing leads to a growth in the amplitude of the Zr–O peak (ordering in the first coordination sphere of metal atoms) and to the appearance of a Zr–Zr peak and the peaks corresponding to ordered oxygen atoms in the subsequent coordination spheres of zirconium.

4. ELECTRON STRUCTURE OF AMORPHOUS ZrO_2 BY UPS, XPS, AND EELS DATA

Figure 4 presents the UPS spectrum (excited by HeI radiation with $E = 21.2$ eV) of the valence band of amorphous ZrO_2 in comparison to the (calibration) spectrum of gold. The low-energy part of the UPS spectrum provides information about the position of the valence band top in amorphous ZrO_2. The work function (i.e., the Fermi level position relative to the vacuum level) in gold is 5.1 eV. According to the UPS spectrum, the top of the valence band of amorphous ZrO_2 is shifted by 2.5 eV toward higher binding energies relative to the Fermi level in gold. Therefore, the top of the valence band (E_v) in amorphous ZrO_2 occurs at 7.6 eV relative to the vacuum electron level. As is known, the Fermi level of gold coincides with E_v(Si), the energy position of the valence band top in silicon. Thus, a barrier for the injection of holes from silicon to amorphous ZrO_2 is about 2.5 eV. The estimate of the hole barrier at the Si/ZrO_2 interface obtained in our study is close to the value (2.3 eV) obtained from the results of internal photoemission and photoconductivity measurements [21]. In [22], the barrier for holes at the Si/ZrO_2 interface was evaluated as 3.15 eV.

The bandgap width for amorphous ZrO_2 was evaluated using the results of EELS measurements at a primary electron beam energy of 200 eV (Fig. 5). In this spectrum, the zero energy indicates the position of the peak of elastically reflected electrons, while negative energies correspond to inelastically reflected electrons. The bandgap width in amorphous ZrO_2 estimated as depicted in Fig. 5 is $E_g = 4.7 \pm 0.4$ eV. For the comparison, E_g values reported for ZrO_2 in the literature amount to 5.4 eV (photoconductivity data) [21], 4.52–4.67 eV (fundamental optical absorption edge) [22], and 5.5 eV (EELS) [23].

Figure 6 shows the XPS spectrum of the valence band of amorphous ZrO_2 (excited by X-ray quanta with $E = 1486.6$ eV). As can be seen, the valence band of ZrO_2 consists of three subbands with approximately equal halfwidths (FWHM) of about 5 eV. The dominating contribution to this spectrum is from the O2*p* states and Zr 4*d* states [24]. The UPS spectrum excited by HeII radiation with $E = 40.8$ eV (Fig. 7) confirms that the dominating contribution to this energy band is due to the O2*p* states and Zr4*d* states.

Figure 8 presents the second derivative of the electron energy loss spectrum measured at a primary electron beam energy of 500 eV. In this experiment, the peaks due to electron energy losses are observed at

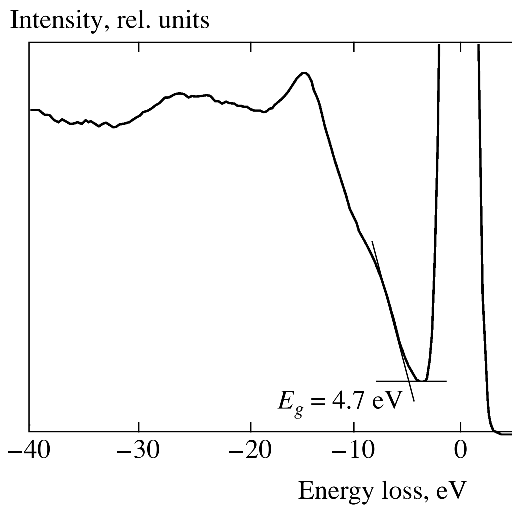

Fig. 5. Electron energy loss spectrum of an amorphous ZrO_2 film (zero loss energy corresponds to the peak of elastically reflected electrons).

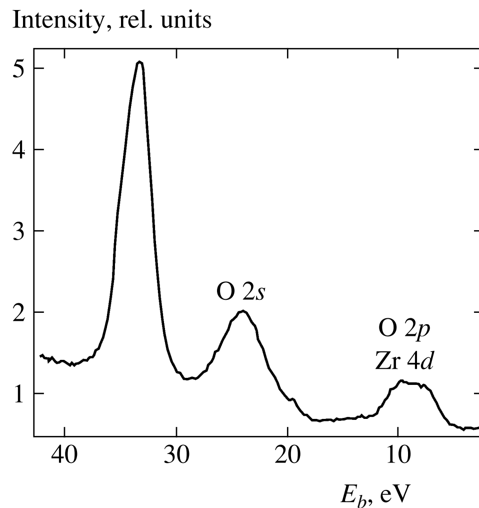

Fig. 6. XPS spectrum of an amorphous ZrO_2 film excited by AlK_α X-ray radiation (E = 1486.6 eV).

14.0, 7.4, and 3.0 eV. The first two peaks observed at energies exceeding the bandgap width of ZrO_2 should be assigned to the interband electron transitions from the valence to conduction band. The energy of the third peak (3 eV) is lower than the bandgap width, which probably implies that this peak is due to the excitation of electron transitions involving levels related to the structural defects in ZrO_2. Foster et al. [25, 26] studied the intrinsic point defects in ZrO_2 and established that the levels of oxygen vacancies are situated at about 3.3 eV. Thus, the transition at 3.0 eV is probably due to the excitation of localized states related to the presence of oxygen vacancies in the ZrO_2 structure.

5. CHARGE TRANSFER IN Si–ZrO_2–Al STRUCTURES

The barrier Φ^e for electrons at the Si/dielectric interface typically falls within 1.0–4.0 eV. In particular, the barrier heights are 2.0 eV for Si/HfO_2 and Si/Al_2O_3 interfaces. According to Afanas'ev et al. [21], the barrier height for Si/ZrO_2 is also Φ^e = 2.0 eV. The effective masses of charge carriers in dielectrics such as SiO_2, Si_3N_4, HfO_2, Al_2O_3, and La_2O_5 typically fall within $m_e^* \approx m_h^* \approx (0.15–0.5)m_0$ [15, 19, 27]. At room temperature, the injection of electrons from a semiconductor (or metal) through the barrier with a height of 2.0 eV proceeds according to the Fowler–Nordheim mechanism and the corresponding current can be expressed as [14]

$$J = \frac{e^3F^2}{16\pi^2\hbar\Phi}\exp\left(\frac{4\sqrt{m^*\Phi^3}}{3\hbar eF}\right).$$

where F is the electric field strength, m^* is the effective mass of carriers, and Φ is the barrier height.

Figure 9 shows the experimental J–U curves for the Si–ZrO_2–Al structure measured for two bias voltage polarities. In both cases, the measurements were performed in the regime of enrichment for the silicon substrate. For the comparison, solid curves in Fig. 9 show the current–voltage characteristics calculated using the Fowler–Nordheim model for the effective tunneling masses of electrons and holes $m_e^* = m_h^* = 0.5m_0$. In

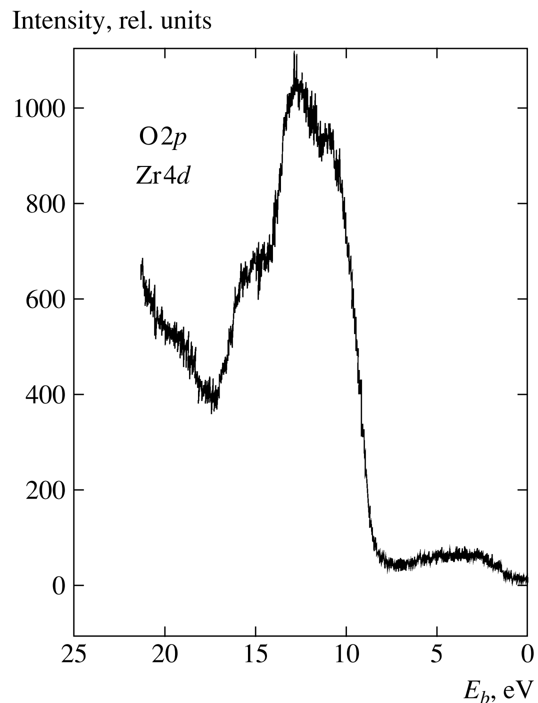

Fig. 7. UPS spectra of an amorphous ZrO_2 film excited by HeII radiation (E = 40.8 eV).

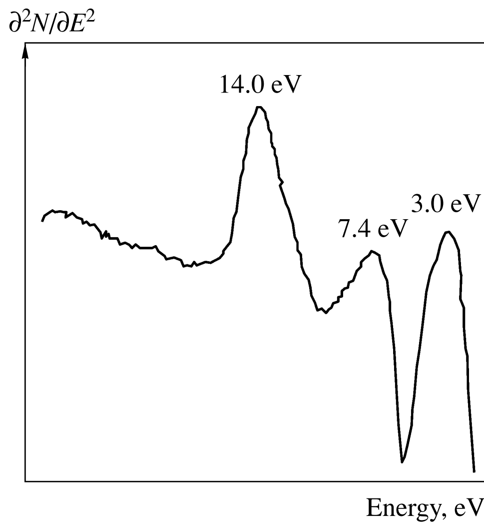

Fig. 8. The second derivative of the electron energy loss spectrum of an amorphous ZrO_2 film measured at a primary electron beam energy of 500 eV.

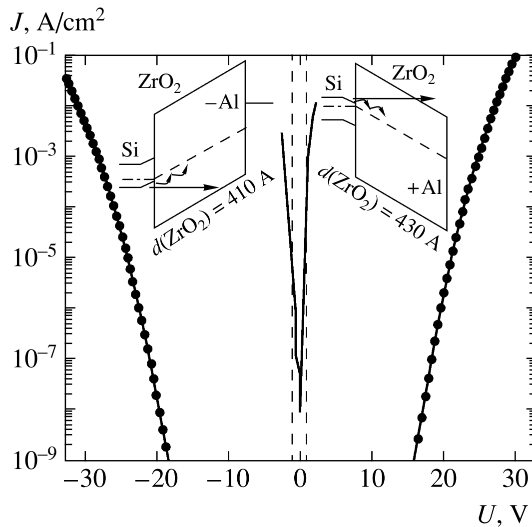

Fig. 9. Current–voltage characteristics of the *n–p* structure Si–ZrO_2–Al measured in the regime of enrichment for two bias voltage polarities (with plus and minus on Al electrode. Points present the experimental data; solid and dashed curves show the results of calculations using the Fowler–Nordheim model for $m_e^* = m_h^* = 0.5m_0$ and $m_e^* = m_h^* = 0.0005m_0$, respectively. The insets illustrate the model of carrier injection via localized states (traps).

calculations for a barrier height of 2.0 eV, the current density $J = 10^{-7}$ A/cm^2 corresponds to the electric field strength $F \approx 0.8 \times 10^6$ V/cm (referred to below as threshold). In experiment, the threshold field strength amounts to 5×10^4 V/cm that implies an anomalously high level of electron and hole injection from silicon and aluminum into ZrO_2. Dashed lines in Fig. 9 present the current–voltage characteristics calculated for Φ^e = 2.0 eV and the effective mass selected so as to provide agreement with experiment. The agreement was obtained only for an anomalously small effective electron mass in ZrO_2: $m_e^* \approx 0.0005m_0$. As will be seen below from the results of electron energy band structure calculations for cubic ZnO_2, the theory does not predict the existence of such anomalously light electrons. It should be noted that minimal effective electron masses reported for well-known crystalline semiconductors amount to $0.01m_0$ [28].

Thus, Si/ZrO_2 and Al/ZrO_2 interfaces feature an anomalously high level of electron injection. It should be noted that anomalously high leakage currents are generally typical of alternative gate dielectrics. In particular, anomalously large currents (manifested by the absence of a threshold on the current–voltage characteristics) were observed in ZrO_2 [29], Ta_2O_5 [30], Y_2O_3, Gd_2O_3 [31], Pr_2O_3 [32], La_2O_3 [33], Sm_2O_3 [34], TiO_2 [35], and $Ba_{0.5}Sr_{0.5}TiO_3$ [36].

In this context, the following circumstances have to be noted:

(i) The currents are measured in the electric fields, which are insufficient for the injection by tunneling from the contact. This fact suggests that electrons are injected from the contacts to certain localized states (traps), rather than directly to the conduction band. Such a model was previously considered in [30, 37].

(ii) The energy of localized states in a dielectric according to this model must be close to the Fermi energy in the contact (see the inset to Fig. 9). In particular, for the Al/ZrO_2 interface, the energy of traps for the electron injection must be about 2.0 eV.

(iii) The values of electric field strengths corresponding to the observed leakage currents are insufficient to provide electron injection to the conduction band, which implies that electrons are transferred via localized states by analogy with the mechanism of hopping transport [38].

Jeon and Hwang [39] studied the current–voltage characteristics of ultrathin (≈50 Å) ZrO_2 films and showed that the annealing of samples in a humid oxygen atmosphere leads to a considerable decrease in the level of injection currents. At the same time, the photoelectron spectra of annealed samples showed a significant decrease in the intensity of signals corresponding to metallic zirconium. This fact is indicative of a significant decrease in the concentration of oxygen vacancies in the annealed films. Foster et al. [25] studied the defects (oxygen vacancies) in ZrO_2 and established that these defects may act as electron traps. These results confirm the above hypothesis that the charge transport in ZrO_2 proceeds via localized states. More detailed

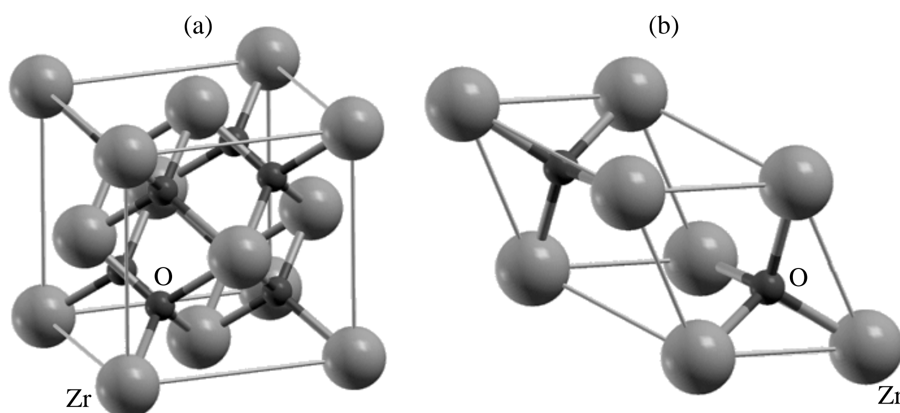

Fig. 10. Schematic diagrams of (a) face-centered cubic and (b) primitive rhombohedral cells of ZrO_2.

investigation into the mechanism of conductivity in ZrO_2 is outside of the scope of this paper.

6. ELECTRON STRUCTURE OF CUBIC ZrO_2: ENERGY BAND CALCULATIONS AND COMPARISON WITH EXPERIMENT

The energy band structure calculations for ZrO_2 were previously performed in [25, 26, 40, 41]. However, no data were reported on the calculation of effective masses of electrons and holes, while the calculated bandgap widths have proved to be significantly lower than experimental values. For this reason, we carried out energy band calculations in order to evaluate the effective masses of charge carriers and refine the bandgap width. The calculations were performed for the cubic modification (c-ZrO_2) containing the minimum number of atoms in the unit cell and, hence, requiring minimum computational facilities. Some papers [10, 11] reported on the predominant formation of a high-temperature cubic phase in thin ZrO_2 films grown at temperatures about 200°C under the conditions of oxygen depletion.

In the cubic ZrO_2 modification, zirconium atoms form a face-centered cubic structure with a lattice parameter of 4.9 Å (Fig. 10a), while oxygen atoms occupy the tetrahedral positions in this lattice. The primitive rhombohedral cell has an edge length of 3.47 Å and contains three atoms with the following coordinates in the crystal coordinate system (Fig. 10b): Zr (0, 0, 0); O1 (0.25, 0.25, 0.25); and O2 (0.75, 0.75, 0.75). All Zr–O distances are equal and amount to 2.1 Å. Figure 11 shows the Brillouin zone and indicates the special points for the primitive rhombohedral cell of ZrO_2.

The electron energy band structure calculations were performed using the density functional approximation with a nonlocal exchange-correlation potential and gradient corrections in the Perdew–Burke–Ernzerhof (PBE) parametrization [42] as realized in the quantum-chemical program packages v-ESPRESSO [43] and ADF-BAND [44–46]. The valence band contained the 4*s*, 4*p*, 4*d*, and 5*s* electron levels of zirconium and 2*s* and 2*p* electron levels of oxygen. The core electrons were taken into account in terms of the ultrasoft pseudo-potentials in the v-ESPRESSO program package and in the approximation of frozen orbitals in the ADF-BAND program package. The former package employed a flat wave basis set [47], while the latter package used a basis set in the form of Slater functions and numerical atomic orbitals calculated using the Herman–Skilmann program. The flat wave basis set functions were truncated at an energy of 30 Ry. Both packages give qualitatively similar and quantitatively close results. Below we present the data obtained using the v-ESPRESSO program package.

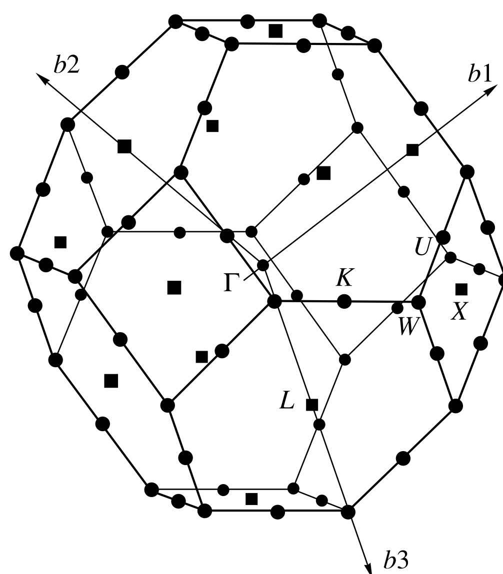

Fig. 11. Schematic diagram of the Brillouin zone and special points of the primitive rhombohedral cell of ZrO_2.

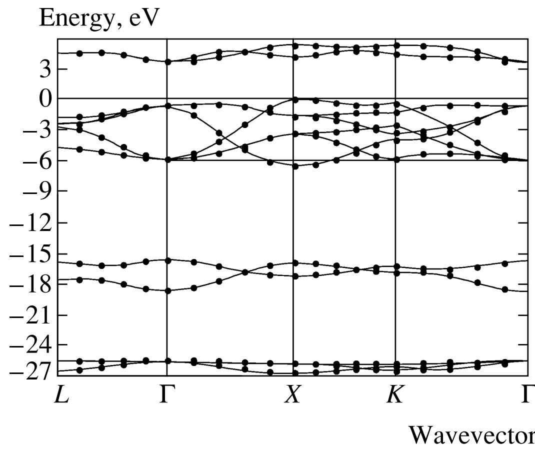

Fig. 12. Theoretical dispersion $E(k)$ along the special points of the Brillouin zone of ZrO_2.

Figure 12 present the pattern of theoretical dispersion constructed along the special points of the Brillouin zone of ZrO_2 (see Fig. 11). The bottom of the conduction band is at point Γ, while the top of the valence band is at point X. Thus, the cubic modification of ZrO_2 is a nondirect-band dielectric.

The bandgap width E_g estimated as an energy difference between the valence band top and the conduction band bottom is about 3.2 eV, which is substantially lower than the experimental values (by various data, 4.7–5.5 eV).

Alternatively, E_g can be evaluated as a difference of the excitation energies for electrons at the conduction band bottom (E_c^{exc}) and at the valence band top (E_v^{exc}):

$$E_g = E_c^{exc} - E_v^{exc}.$$

In order to estimate E_c^{exc} and E_v^{exc}, we calculated the total energy of the neutral cell (E_0) and the cells containing additional electron (E_e) and hole (E_h) [48]:

$$E_c^{exc} = E_e - E_0, \quad E_v^{exc} = E_0 - E_h,$$

$$E_g = E_e + E_h - 2E_0.$$

The total energies of the cells containing additional electron and hole were calculated by introducing a compensating charge smeared over the cell. The cell with additional electron or hole becomes a metallic system that may require a greater number of k-points for the correct calculation. In order to estimate the error related to this circumstance, we calculated the total energies E_0, E_e, and E_h on the 24 × 24 × 24 (256 k-points) and 16 × 16 × 16 (145 k-points). The difference of the corresponding total energies was below 10^{-4} Ry. The resulting estimate for the bandgap width was E_g = 5.2 eV, which is close to the experimental value (4.7 ± 0.5 eV) obtained in this study for amorphous ZrO_2 films. In calculating E_g according to the procedure described above, we used the following simplifying assumptions: (i) the Coulomb interaction between electron and hole was ignored and (ii) the total energy of a charged cell was calculated assuming that the additional charge (electron or hole) is localized within the unit cell.

Table 1. Effective electron masses at point Γ of the Brillouin zone

Direction in the Brillouin zone	$(m_e^*)_1/m_0$	$(m_e^*)_2/m_0$
Γ–X	2.01	0.58
Γ–L	0.78	0.78
Γ–K	1.25	0.64

Figure 13a shows the dispersion $E(k)$ for electrons at the bottom of the conduction band. Point Γ represents a doubly degenerate state, which splits in the Γ–X and Γ–K directions and remains degenerate in the Γ-L direction. The effective electron masses m_e^* corresponding to this law of dispersion were calculated as

$$m_e^* = \frac{\Delta k^2}{2\Delta E},$$

where ΔE is the energy difference between point Γ and the point occurring at a distance of Δk in the corresponding direction in the reciprocal space. The effective electron masses determined using this method are presented in Table 1. The results of calculations show that the m_e^* values for various directions in the Brillouin zone fall within $(0.6–2.0)m_0$ (see Table 1). Thus, the assumption concerning the existence of anomalously light electrons with $m_e^* \approx (10^{-4}–10^{-3})m_0$ in ZrO_2, which was made for the interpretation of data on the conductivity, is not confirmed by the results of band calculations.

Figure 13b shows the dispersion $E(k)$ for holes in the vicinity of point X. Table 2 gives the effective masses of holes calculated using a method analogous to that described above for electrons. The results of these calculations show that ZrO_2 contains both heavy ($m_h^* \approx 3.5m_0$) and light ($m_h^* \approx 0.3m_0$) holes.

Figure 14 presents the calculated partial densities of states for the 4p and 4d levels of zirconium and the 2s and 2p levels of oxygen, as well as the total density of states. Here, the energies are measured from the top of the valence band. In these calculations, we took into account the Gaussian broadening (with a width of 025 eV). The results of these calculations show that the contributions from 4s, 5s, and 5p states of zirconium to all three valence subbands are negligibly small (these partial contributions to the density of states are not

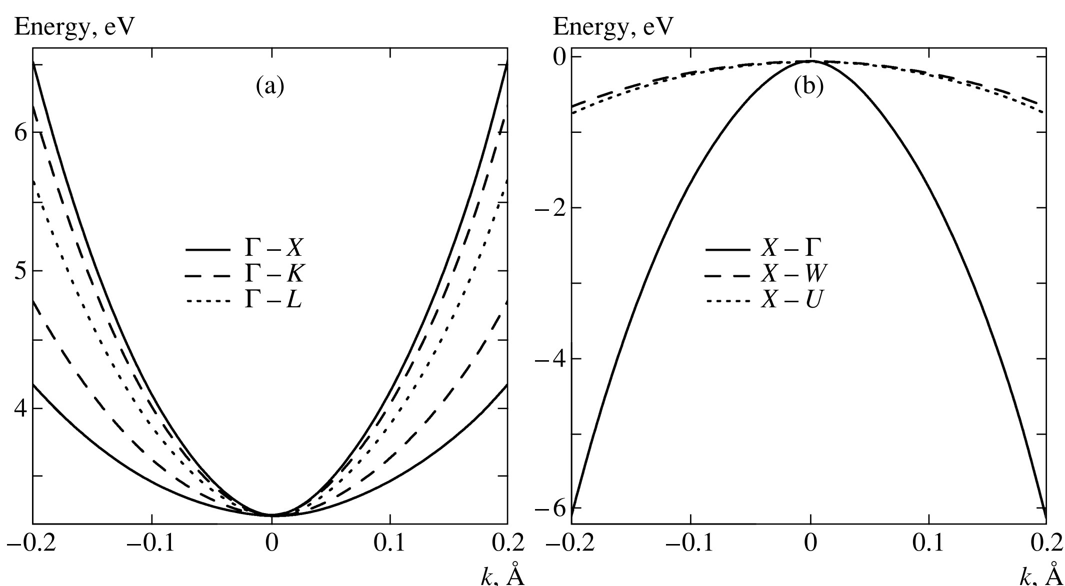

Fig. 13. The laws of dispersion $E(k)$ for (a) electrons in the vicinity of point Γ and (b) holes in the vicinity of points X.

depicted in Fig. 14). According to these results, the lower subband is formed virtually completely by the Zr4p states, while the middle subband is formed by the O2s states with a small admixture of the Zr4d states (only the 4d functions with xy, xz, and yz symmetry make these contributions). The upper subband is formed by the O2p states, also with an admixture of the Zr4d states (xy, xz, yz, $x^2 - y^2$, and z^2 functions), and the conduction band is formed predominantly by the Zr4d states.

The charge transfer along the Zr–O bond, as estimated from the analysis of populations according to Levdin, amounts to 0.1e. Accordingly, zirconium atom bears a positive charge $\Delta q = 0.8e$, oxygen atom has a negative charge $\Delta q = -0.4e$, and the Zr–O bond has an ionic–covalent character.

A comparison of the total density of states with the valence-band photoelectron spectrum obtained for E = 1486.6 eV shows a good qualitative agreement (cf. Figs. 6 and 14). As can be seen, there are three subbands separated by the ionic gap. However, this comparison reveals a difference in the widths of peaks in the total density of states, where the two low-energy peaks are with FWHM ~ 1.5 and 2.5 eV), in contrast to the peaks in the experimental spectra (with FWHM ~ 5 eV). This discrepancy can be related to a finite lifetime of holes on the core levels, which leads to the broadening of experimental peaks. The adequate analysis of factors (in particular, Auger processes) responsible for the broadening of peaks requires a more complicated model and is outside of the scope of this paper.

7. DISCUSSION OF RESULTS

The vacuum annealing of as-deposited amorphous ZrO_2 films at 800°C leads to the formation of a high-temperature cubic phase. According to the published data, the equilibrium temperature of c-ZrO_2 formation is 2600 K. Thus, thin films admit the formation of non-equilibrium crystalline phases, and this circumstance can significantly influence the characteristics of dielectric films.

The results of our EELS measurements show the presence of a peak at an energy of 3.0 eV, which is below the bandgap width (~4.7 eV) in ZrO_2. The energy losses of about 3.0 eV can be related to the excitation of electron transitions involving the structural defects in ZrO_2, most probably, oxygen vacancies. This conclusion is confirmed by the published theoretical results [25, 26] and by our calculations for the oxygen vacancies in ZrO_2.

The results of conductivity measurements for the ZrO_2 films in Si–ZrO_2–Al structures showed evidence for an anomalously high level of electron injection at the Si/ZrO_2 and Al/ZrO_2 interfaces. It should be noted that high leakage currents are typical of most alternative gate dielectrics, rather than of particular samples. In order to interpret the anomalously high conductivity within the framework of a simple model of electron injection from a semiconductor (or metal) by tunneling

Table 2. Effective hole masses at point X of the Brillouin zone

Direction in the Brillouin zone	m_h^*/m_0
X–Γ	0.32
X–U	2.64
X–W	3.05

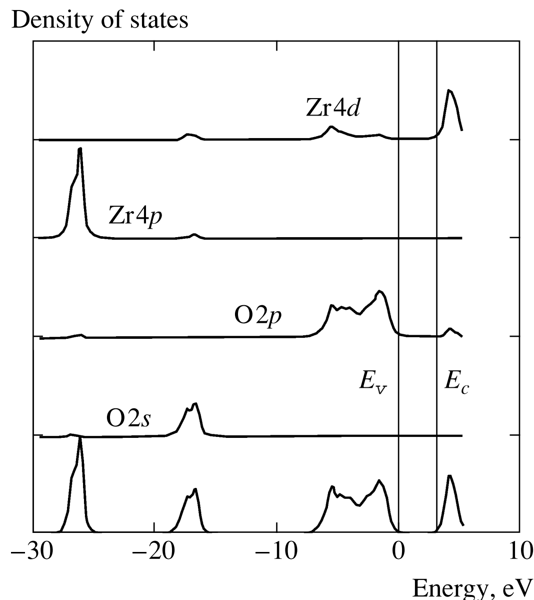

Fig. 14. Calculated partial densities of Zr (4*p* and 4*d*) and O (2*s* and 2*p*) states and the total density of states (bottom curve).

according to the Fowler–Nordheim mechanism via the barrier with a height of about 2.0 eV, it is necessary to assume the existence of carriers with a nonphysically small effective mass of $m_e^* \approx 0.0005m_0$, which is not confirmed by the results of band calculations. In order to explain the observed anomalous conductivity, we put forward a hypothesis, whereby the electrons are transferred via localized states by a mechanism similar to that of hopping conductivity [38].

The energy band structure calculations performed using the density functional method for a cubic ZrO_2 phase yield a valence band structure qualitatively coinciding with the experimental data provided by photoelectron spectroscopy. The theoretically calculated bandgap width (5.2 eV) is close to the experimental value (4.7 eV).

We have theoretically calculated for the first time the effective masses of electrons and holes for the cubic ZrO_2 phase. The effective masses of electrons for various directions in the Brillouin zone fall within $(0.6–2.0)m_0$. Therefore, the assumption concerning the existence of anomalously light electrons with $m_e^* \approx (10^{-4}–10^{-3})m_0$ (that was necessary for the interpretation of conductivity data within the framework of the conventional model) is not conformed by the band structure calculations. Our calculations showed that both heavy ($m_h^* \approx 3.5m_0$) and light ($m_h^* \approx 0.3m_0$) holes exist in ZrO_2, depending on the direction in the Brillouin zone. The substantial anisotropy of the effective electron and hole masses in ZrO_2 can be used to suppress the injection of carriers in silicon by growing ZrO_2 films with the corresponding orientation.

ACKNOWLEDGMENTS

This study was supported by the Siberian Division of the Russian Academy of Sciences (integration project no. 116), the Ministry of Education and Science of the Russian Federation (project no. 02.435.11.2002), the Research Grants Council of Hong Kong (UGC Competitive Earmarked Research Grant No. CityU 1167/03E), and the Korean Ministry of Science and Technology within the framework of the National Tera-Level Nanodevice Program.

REFERENCES

1. A. I. Kingon, J.-P. Maria, and S. K. Streiffor, Nature **406**, 1032 (2000).
2. G. D. Wilk, R. M. Wallace, and J. M. Anthony, J. Appl. Phys. **89**, 5243 (2001).
3. J. Robertson, Eur. Phys. J.: Appl. Phys. **28**, 265 (2004).
4. V. A. Gritsenko, K. A. Nasyrov, Yu. N. Novikov, et al., Solid-State Electron. **47**, 1651 (2003).
5. V. A. Gritsenko, K. A. Nasyrov, D. V. Gritsenko, et al., Fiz. Tekh. Poluprovodn. (St. Petersburg) **39**, 748 (2005) [Semiconductors **39**, 716 (2005)].
6. V. A. Gritsenko, *Atomic and Electronic Structure of Amorphous Dielectrics in Silicon MIS Devices* (Nauka, Novosibirsk, 1993) [in Russian].
7. V. A. Gritsenko, in *Silicon Nitride in Electronics* (Elsevier, New York, 1988), p. 263.
8. C. J. Howard, R. J. Hill, and B. E. Reichert, Acta Crystallogr. B **44**, 116 (1988).
9. E. Ryshkewitch and D. W. Richerson, *Oxide Ceramics. Physical Chemistry and Technology* (Academic, Orlando, 1985).
10. J. P. Holgado, J. P. Espinos, F. Yubero, et al., Thin Solid Films **389**, 34 (2001).
11. J. Aarik, A. Aidla, H. Mandar, et al., Thin Solid Films **408**, 97 (2002).
12. R. R. Manory, T. Mori, I. Shimuzu, et al., J. Vac. Sci. Technol. A **20**, 549 (2002).
13. J. Schaefer, N. V. Edwards, R. Liu, et al., J. Electrochem. Soc. **150** (4), 67 (2003).
14. S. M. Sze, *Physics of Semiconductor Devices*, 2nd ed. (Wiley, Taiwan, Taipei, 1985; Mir, Moscow, 1984), p. 868.
15. V. A. Gritsenko, E. E. Meerson, and Yu. N. Morokov, Phys. Rev. B **57**, 2081 (1997).
16. P. M. Schneider and W. B. Fowler, Phys. Rev. Lett. **36**, 425 (1976).
17. J. R. Chelikowsky and M. Shluter, Phys. Rev. B **15**, 4020 (1977).
18. Y.-N. Xu and W. Y. Ching, Phys. Rev. **23**, 5454 (1981).
19. S. Zafar, K. A. Conrad, Q. Liu, et al., Appl. Phys. Lett. **67**, 1031 (1995).

20. N. Binsted, J. W. Campbell, S. J. Gurman, and P. C. Stephenson, SERC Daresbury Lab. Rep. (1991).
21. V. V. Afanas'ev, M. Houssa, A. Stesmans, and M. M. Heyns, J. Appl. Phys. **91**, 3079 (2002).
22. S. Venkataraj, O. Kappertz, H. Weis, et al., J. Appl. Phys. **92**, 3599 (2002).
23. S. Miyazaki, M. Narasaki, M. Ogasawara, and M. Hirose, Microelectron. Eng. **59**, 373 (2001).
24. J.-J. Yeh, *Atomic Calculation of Photoionization Cross-Sections and Asymetry Parameters* (Gordon and Breach, Langhorne, PA, 1993), p. 31.
25. A. S. Foster, V. B. Sulimov, F. Lopez-Gejo, et al., Phys. Rev. B **64**, 224108 (2001).
26. A. S. Foster, V. B. Sulimov, F. Lopez-Gejo, et al., J. Non-Cryst. Solids **303**, 101 (2002).
27. Y.-C. Yeo, T.-J. King, and C. Hu, Appl. Phys. Lett. **81**, 2091 (2002).
28. I. M. Tsidil'kovskiĭ, *Electrons and Holes in Semiconductors* (Nauka, Moscow, 1972) [in Russian].
29. K. Kukli, M. Ritala, J. Aarik, et al., J. Appl. Phys. **92**, 1833 (2002).
30. M. Houssa, M. Tuominen, M. Nali, et al., J. Appl. Phys. **87**, 8615 (2000).
31. J. Kwo, M. Hong, A. R. Kortan, et al., J. Appl. Phys. **89**, 3920 (2001).
32. A. Sakai, S. Sakashita, M. Sakashita, et al., Appl. Phys. Lett. **85**, 5322 (2004).
33. J.-P. Maria, D. Wicaksana, and A. I. Kingon, J. Appl. Phys. **90**, 3476 (2001).
34. D. Yang, Li Jue Xue, and R. Devine, J. Appl. Phys. **93**, 9389 (2003).
35. V. Mikhelashvili and G. Eidenstein, J. Appl. Phys. **89**, 3256 (2000).
36. Ki H. Yoon, J. C. Lee, J. Park, et al., Jpn. J. Appl. Phys. **40**, 5497 (2001).
37. A. V. Chaplik and M. V. Éntin, Zh. Éksp. Teor. Fiz. **67**, 208 (1974) [Sov. Phys. JETP **40**, 106 (1974)].
38. B. I. Shklovskiĭ and A. L. Éfros, *Electronic Properties of Doped Semiconductors* (Nauka, Moscow, 1979; Springer, New York, 1984).
39. S. Jeon and H. Hwang, J. Vac. Sci. Technol. B **20**, 400 (2002).
40. G. Jomard, T. Petit, A. Pasturel, et al., Phys. Rev. B **59**, 6 (1999).
41. R. H. French, S. J. Glass, F. S. Ohuchi, et al., Phys. Rev. B **49**, 8 (1994).
42. J. P. Perdew, K. Burke, and M. Ernzerhof, Phys. Rev. Lett. **77**, 3865 (1996).
43. S. Baroni, A. Dal Corso, S. de Gironcoli, et al., http://www.pwscf.org/.
44. G. te Velde and E. J. Baerends, Phys. Rev. B **44**, 7888 (1991).
45. G. Wiesenekker and E. J. Baerends, J. Phys.: Condens. Matter **3**, 6721 (1991).
46. BAND2004.01, SCM, Theoretical Chemistry (Vrije Univ., Amsterdam), http://www.scm.com.
47. D. Vanderbilt, Phys. Rev. B **41**, 7892 (1990).
48. S. T. Pantelides, D. J. Mickish, and A. B. Kubz, Phys. Rev. B **10**, 5203 (1974).

Translated by P. Pozdeev

SPELL: 1. Asymetry—m/b Asymmetry—?